

Substituent-Induced Reactivity in Quinonoid-Bridged Dinuclear Complexes: Comparison between the Ruthenium and Osmium Systems

Michael G. Sommer,^{†,§} David Schweinfurth,^{‡,§} Fritz Weisser,[‡] Stephan Hohloch,[‡] and Biprajit Sarkar^{*,‡}

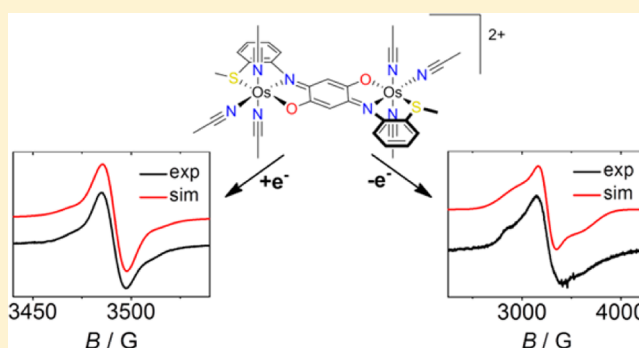
[†]Institut für Anorganische Chemie, Universität Stuttgart, Pfaffenwaldring 55, D-70569 Stuttgart, Germany

[‡]Institut für Chemie und Biochemie, Anorganische Chemie, Fabbeckstraße 34-36, D-14195 Berlin, Germany

Supporting Information

ABSTRACT: The ligand 2,5-bis[2-(methylthio)anilino]-1,4-benzoquinone (L) was used in its doubly deprotonated form to synthesize the complex $[\{\text{Cl}(\eta^6\text{-Cym})\text{Os}\}_2(\mu\text{-}\eta^2\text{-}\eta^2\text{-L}_{2\text{H}})]$ (**1**; Cym = *p*-cymene = 1-isopropyl-4-methylbenzene). Spectroscopic characterization and elemental analysis confirms the presence of the chloride ligands in **1**, which indirectly shows that the bridging ligand $\text{L}_{2\text{H}}$ acts in a bis-bidentate fashion in **1**, with the thioether substituents on the bridge remaining uncoordinated. Abstraction of the chloride ligands in **1** by AgBF_4 in CH_3CN leads not only to the release of those chloride ligands but also to a simultaneous substituent-induced release of Cym with the bridging ligand changing its coordination mode to bis-tridentate. In the resulting complex

$[\{(\text{CH}_3\text{CN})_3\text{Os}\}_2(\mu\text{-}\eta^3\text{-}\eta^3\text{-L}_{2\text{H}})]^{2+}$ (**2**²⁺), the thioether groups of $\text{L}_{2\text{H}}$ are now coordinated to the osmium centers with the bridging ligand coordinating to the metal center in a bis-meridional form. The coordination mode of $\text{L}_{2\text{H}}$ in **2**²⁺ was confirmed by single-crystal X-ray diffraction data. A structural analysis of **2**²⁺ reveals localization of double bonds within the “upper” and “lower” parts of the bridging ligand in comparison to bond distances in the free ligand. Additionally, the binding of the bridge to the osmium centers is seen to occur through O^- and neutral imine-type N donors. The complexes **1** and **2**²⁺ were investigated by cyclic voltammetry and UV–vis–near-IR and EPR spectroelectrochemistry. This combined approach was used to unravel the redox-active nature of the ligand $\text{L}_{2\text{H}}$, to determine the sites of electron transfer (ligand radical versus mixed valency), and to compare the present systems with their ruthenium analogues **3** and **4**²⁺ (Schweinfurth, D. et al. *Inorg. Chem.* **2011**, *50*, 1150). The effect of replacing ruthenium by its higher homologue osmium on the reactivity and the electrochemical and spectroscopic properties were explored, and the differences were deciphered by taking into account the intrinsic dissimilarities between the two homologues. The usefulness of incorporating additional donor substituents on potentially bridging quinonoid ligands was probed in this work.



INTRODUCTION

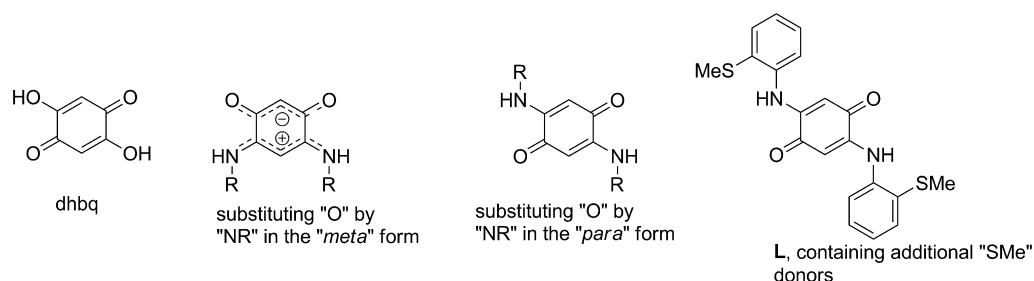
Quinones as redox-active compounds are fascinating ligands in coordination and organometallic chemistry.¹ The ability of quinones and related ligands to exist in various redox forms and, hence, to undergo a series of electron and charge transfer processes has long attracted synthetic and physical inorganic chemists to these systems.² Recent developments have involved the use of quinones as electron reservoirs in their metal complexes to perform small-molecule activation and catalysis.³ The prototype of a quinone ligand capable of bridging two metal centers is 1,4-dihydroxy-2,5-benzoquinone (dwbq; Scheme 1). This all oxygen donor containing ligand has been extensively used in coordination chemistry, and its metal complexes show many interesting properties.⁴ We⁵ and others⁶ have argued in recent years that the tuning of steric and electronic properties of ligands such as dwbq is best achieved by using the [NR] for [O] isoelectronic relationship. On doing

that, we can generate new ligands where the properties of the metal complexes can be easily varied by using the handle “R” on the [NR] groups. Using this concept, we have reported on synthetic strategies for generating a host of “*meta*”^{5a} and “*para*”^{5b,c} forms of ligands derived from dwbq, where two of the [O] groups have been replaced by [NR] groups (Scheme 1).

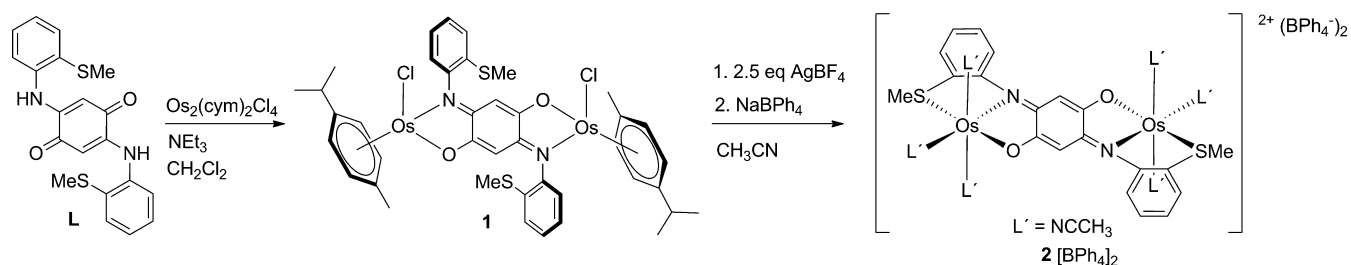
Such ligands have been used by us and others for generating metal complexes with the goal of studying electron transfer,^{5,7} magnetism,^{5b,8} metal–metal coupling,^{7a–g} homogeneous catalysis,⁹ and supramolecular interactions.^{6c,10} Ruthenium complexes with quinone and other ligands have been at the forefront of studies on electron transfer and mixed valency.⁷ One interesting aspect that we observed during the course of developing synthetic routes to such ligands is the ease of

Received: October 6, 2012

Scheme 1. Modification of Potentially Bridging Quinones: from [O,O,O,O] through [O,N,O,N] to a Ligand with Additional Donors on the Nitrogen Substituents



Scheme 2. Synthesis of Diosmium Complexes 1 and 2[BPh₄]₂



introducing an additional donor group in the handle “R” in [NR].^{5c} Such a group can be a donor atom capable of coordinating on demand during a chemical process and, hence, acting as a hemilabile group.¹¹ Reports of potentially bridging quinone ligands with additional donating groups on the substituents remain rare in the literature.^{6c,9e} In the present study we have used the ligand L (L = 2,5-bis[2-(methylthio)anilino]-1,4-benzoquinone) to generate the complexes [$\{\text{Cl}(\eta^6\text{-Cym})\text{Os}\}_2(\mu\text{-}\eta^2\text{-}\eta^2\text{-L}_{2\text{H}})\text{]}^{2+}$ (**1**) and [$\{(\text{CH}_3\text{CN})_3\text{Os}\}_2(\mu\text{-}\eta^3\text{-}\eta^3\text{-L}_{2\text{H}})\text{]}^{2+}$ (**2**²⁺). By using the same ligand, we were able to show that the initially formed complex [$\{\text{Cl}(\eta^6\text{-Cym})\text{Ru}\}_2(\mu\text{-}\eta^2\text{-}\eta^2\text{-L}_{2\text{H}})\text{]}$ (**3**; Cym = *p*-cymene = 1-isopropyl-4-methylbenzene) releases its Cym ligands as a result of chloride abstraction and thioether coordination in an unprecedented reaction, resulting in the formation of [$\{(\text{CH}_3\text{CN})_3\text{Ru}\}_2(\mu\text{-}\eta^3\text{-}\eta^3\text{-L}_{2\text{H}})\text{]}^{2+}$ (**4**²⁺).^{5c}

We discuss here the role that the thioether group plays in displacing the Cym ligand on going from **1** to **2**²⁺ and compare the reaction times and reactivity patterns of the ruthenium complexes **3** and **4**²⁺^{5c} with those of their osmium-containing homologues **1** and **2**²⁺. Investigations of the complexes through single-crystal X-ray diffraction studies, electrochemistry, and UV–vis–near-IR and EPR spectroelectrochemistry will be reported. The complexes will be discussed with respect to their reactivity and structural, electrochemical, and spectroelectrochemical properties with focus on the effects brought about by replacing ruthenium with osmium. It should be noted here that reports on dinuclear complexes of osmium with bridging ligands in general, and quinone bridges in particular, are rare in the literature in comparison to their ruthenium counterparts.¹² Reasons for this are the often tricky synthesis of osmium complexes in comparison to their ruthenium analogues. In this report we present the synthesis and detailed structural, electrochemical, and spectroscopic characterization of two well-defined dinuclear osmium complexes.

RESULTS AND DISCUSSION

Synthesis, Characterization, and Crystal Structure of 2²⁺. The ligand L was prepared by a route recently reported by

us.^{5c} Complex **1** was synthesized by reacting [$\{(\text{Cym})\text{-ClOs}\}_2(\mu\text{-Cl})\text{]}^{13}$ with L in the presence of a base at room temperature (Scheme 2). This reaction worked in a straightforward manner, with no complicated purification steps required, and resulted in a product yield of 85% (Experimental Section). The yield and the reaction conditions are very similar to those we recently reported for **3**.^{5c}

In the ¹H NMR spectrum of **1**, the signals corresponding to the alkyl and the aryl protons of the Cym ligand are found in the expected region (Experimental Section). Additionally, the signal corresponding to the methyl groups of SMe appears at 2.58 ppm. This is very similar to the value of 2.45 ppm found for the same protons in the free ligand.^{5c} The C–H ring proton of the substituted quinone ring appears at 4.93 ppm; the corresponding value for the ruthenium analogue **3** is 4.78 ppm.^{5c} In the mass spectrum a peak corresponding to [**1** – 2Cl]²⁺ was observed. Elemental analysis data match perfectly with the formulation of **1**. All these data point to the presence of the chlorides as well as the Cym ligands in **1**. Thus, it can be concluded that the ligand L_{2H} acts in a bis-bidentate fashion in **1**, coordinating to the osmium center through the oxygen and nitrogen atoms. The complex **1** can in principle exist in the *syn* or *anti* form (it is the orientations of the Cym and chloride ligands that define *syn* or *anti*). Despite several attempts, we were not able to grow crystals suitable for single-crystal X-ray diffraction analysis. Hence, we cannot comment on the configuration around the metal centers in **1** with certainty. However, we note that, in the ruthenium analogue **3**, the molecule with the chloride ligands in *syn* positions had preferentially crystallized.^{5c} In the present case for **1**, the ¹H NMR spectrum clearly showed the formation of a single isomer (Figure S1, Supporting Information).

We next tried to use AgBF₄ to abstract the chloride ions from **1**. Such a procedure has been used by several groups to generate solvent-coordinated (substitution of Cl[−] with solvent molecules), quinone-bridged, dinuclear complexes with d⁶ metal centers, which are reacted with additional bridging ligand, leading to solvent displacement and formation of

molecular squares.^{46,10} All such ligands usually contain no additional donor atoms other than those directly bound to the quinone ring (usually acting as a bis-bidentate ligand). In the present case, ¹H NMR analyses of the product formed after chloride abstraction showed no trace of signals corresponding to the Cym protons (Figure S2, Supporting Information). The SMe protons, which appear at 2.45 and 2.58 ppm, respectively, for **L**^{5c} and **1**, show up at 2.87 ppm for this new product. The C–H quinone ring proton is seen at 6.92 ppm. Additionally, two sets of signals (axial and equatorial) corresponding to coordinated acetonitrile are observed between 2.42 and 2.44 ppm and at 2.71 ppm. These data point to the release of Cym during the chloride abstraction process, and the coordination of the thioether groups (uncoordinated in **1**) and of acetonitrile molecules to the metal centers. Mass spectral analysis of the product also confirmed the formation of a Cym-free compound (Experimental Section). Having established the similar nature of the ruthenium and osmium compounds, a look at reaction conditions points to some differences in the two cases. Whereas the conversion of **3** to **4**²⁺ required only 3 h of reflux in acetonitrile and led to 85% product formation,^{5c} the reaction of **1** to give the new product **2**²⁺ required 19 h of reflux in acetonitrile and delivered the product in only 22% yield (Experimental Section). Osmium is known to form much stronger bonds to ligands in comparison to ruthenium.¹² This would explain the need for much longer reaction times in the present case in comparison to what we have reported for the ruthenium compounds. Such drastic conditions probably also lead to the generation of more byproducts, which decrease product yields. Similar problems with the synthesis of osmium compounds are known in the literature.

Final proof of the composition of the product **2**²⁺, formed after chloride abstraction from **1**, came from a structure determination through single-crystal X-ray diffraction analysis. Anion exchange (BPh₄⁻ for BF₄⁻) was necessary to obtain good-quality single crystals for this compound (Experimental Section). 2[BPh₄]₂ crystallizes with two toluene solvate molecules in the triclinic *P* $\bar{1}$ space group (Table S1, Supporting Information). One of the toluene solvent molecules is highly disordered at the measurement temperature of 100 K.

Each of the osmium centers in **2**²⁺ is coordinated in a distorted-octahedral environment by the O, N, and S donors of the ligand **L**_{2H} and three acetonitrile molecules (Figure 1). The distortion is imposed by the chelating nature of the ligand **L**_{2H}. The molecule has a local center of inversion, making the halves

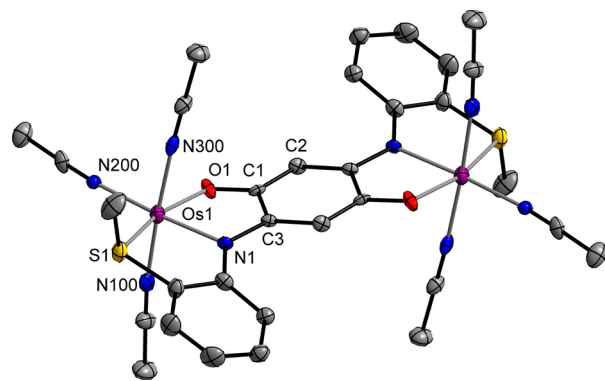


Figure 1. ORTEP plot of 2[BPh₄]₂·2C₇H₈. Ellipsoids are drawn at the 50% probability level. Toluene and tetraphenylborate molecules have been omitted for clarity.

equivalent to each other. The Os1–S1 distance of 2.283(1) Å lies in the range of an authentic bond. The S atom of the SMe group is thus coordinated to the osmium center in **2**²⁺. The bridging ligand binds to each of the osmium centers in a bis-tridentate form with the O, N, and S atoms at each metal center coordinating in a meridional (*mer*) fashion. The remaining three coordination sites are taken up by the acetonitrile molecules. A look at the bond lengths within the quinone ligand in **2**²⁺ and a comparison of these with the bond lengths of the free ligand and of **4**²⁺^{5c} show some interesting trends (Table 1). The C1–O1 bond length of 1.309(6) Å in **2**²⁺ is

Table 1. Bond Lengths (in Å)

| | L | 4 ²⁺ | 2 ²⁺ |
|--------|----------|------------------------|------------------------|
| C1–C2 | 1.432(2) | 1.383(7) | 1.385(7) |
| C2–C3 | 1.365(2) | 1.392(9) | 1.400(7) |
| C1–C3 | 1.524(2) | 1.50(1) | 1.488(6) |
| C1–O1 | 1.233(2) | 1.288(8) | 1.309(6) |
| C3–N1 | 1.344(2) | 1.335(6) | 1.360(6) |
| M–O1 | | 2.076(4) | 2.078(4) |
| M–N1 | | 2.017(5) | 2.009(4) |
| M–S1 | | 2.289(2) | 2.283(1) |
| M–N100 | | 2.013(5) | 2.012(5) |
| M–N200 | | 2.051(6) | 2.022(4) |
| M–N300 | | 2.005(5) | 1.999(5) |

longer than that in the free ligand **L** at 1.233(2) Å. The C1–C2 bond at 1.385(7) Å is, however, shorter than 1.432(2) Å for the same bond in **L**. The C2–C3 bond lengths for **2**²⁺ and **L** are 1.400(7) and 1.365(2) Å, respectively, showing a reasonable elongation of this bond on metal coordination. Thus, whereas in the free ligand **L** the bonds are largely delocalized in the “upper” and “lower” parts of the molecule, metal coordination seems to localize these bonds. Thus, the coordination of the ligand is best described through an O⁻ type donor and an imine type neutral nitrogen N donor. The short C1–C2 bond next to the C–O bond and the slightly longer C2–C3 bond next to the C–N bond would support this hypothesis. Coordination through an O⁻ donor and a neutral N donor was also observed for **4**²⁺ and for other complexes containing similar ligands. The more electronegative O atom apparently is better suited to stabilize the negative charge.^{5b,c,7c,g} The C1–C3 bond which connects the “upper” and “lower” parts of the quinone ligand remains a long single bond in **L**, **2**²⁺, and **4**²⁺ (Table 1).

The quinone ring and the O and N donor atoms are largely planar. However, the two thioether groups are displaced out of the plane with a dihedral angle of 24.5(2)° between the quinone OCCN and NCCS planes in **2**²⁺. The corresponding dihedral angle for **4**²⁺ is 26.3(2)°.^{5c} The intramolecular Os–Os distance in **2**²⁺ is 7.8501(8) Å. The corresponding distance in the ruthenium complex **4**²⁺ is 7.8533(8) Å.^{5c}

Comments on the Release of Cym from **1 To Form **2**²⁺.** The processes of chloride abstraction, thioether and acetonitrile coordination, and Cym release from **1** to produce **2**²⁺ seem to be strongly correlated. Reports by us^{5c} and others^{46,10} have proven that it is possible to abstract chloride atoms from related complexes that contain no additional donor atoms in the bridging quinones and generate solvent-substituted complexes that still have Cym as ligands. The detection of the [**1** – 2Cl]²⁺ peak in the mass spectrometric experiments with **1** shows that a simple chloride abstraction is not enough for Cym release and thioether coordination in the

gas phase. Treatment of **1** with 2 equiv of Ag^+ triggers a sequence of consecutive events. Chloride abstraction from osmium increases the Lewis acidity of the metal ions, which can be met by binding of the dangling thioether donors. The Cym ligand bound to osmium in a η^6 fashion requires that the other three donor atoms bind to the metal center in a facial (*fac*) form.¹⁴ This, however, requires a large amount of bending around various bonds with partial double-bond character. The bridging ligand is not flexible enough to allow for the corresponding distortion. Thus, the energetically feasible way for the ligand to bind with all of its O, N, and S donors to the metal center is in a *mer* form. However, once the bridging quinone binds to the metal center in a *mer* form, the coordination of Cym is no longer possible. The Cym ligands are thus released from the molecule with concomitant coordination of the corresponding number of acetonitrile donors.

The necessity of such a donating solvent is clear from mass spectrometric experiments of **1**, where despite chloride abstraction and a possible increase in the Lewis acidity of the metal center, no Cym release occurs in the gas phase. Attempts to perform the reaction of **1** with a Ag^+ source in dichloromethane/toluene in order to generate a coordinatively unsaturated metal complex where each osmium center would have 16 valence electrons were not successful.

Electrochemistry. The presence of a redox-active bridging ligand, together with two redox-active metal centers, makes the complexes reported herein ideal candidates for probing their redox properties. The complex **1** shows a reversible oxidation at 0.37 V and an irreversible reduction step at -1.51 V (Figure 2) in $\text{CH}_2\text{Cl}_2/0.1$ M Bu_4NPF_6 .

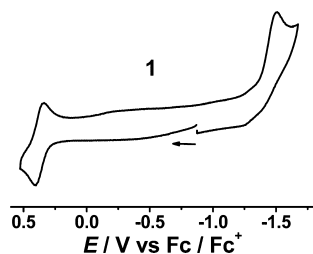


Figure 2. Cyclic voltammogram of **1** in $\text{CH}_2\text{Cl}_2/0.1$ M Bu_4NPF_6 at 295 K.

For comparison, **3**, which contains ruthenium centers instead of osmium, showed only ill-defined, irreversible processes under identical conditions. Quinoidally bridged arene–ruthenium complexes are known to show irreversible electrochemical responses.¹⁵ Reasons for this are the labile ruthenium–chloride bonds, which are highly susceptible to cleavage following redox processes. For **1**, which contains the higher homologue osmium, the metal–ligand bonds are intrinsically stronger; this is a well-known effect on moving down in a group in the periodic table. A consequence of such robust bonds is the reversibility of the oxidation step in **1**. The reduction is irreversible, probably because of chloride dissociation after reduction of complex **1**. Such chloride splitting following reduction has been observed before for arene-containing complexes of a d^6 metal center with redox-active ligands.¹⁶

For the cymene-free ruthenium complex 4^{2+} we had made an error in referencing in our earlier report.^{5c} The correct potentials for this complex are given in Table 2, and an

Table 2. Electrochemical Potentials of the Complexes^a

| compd | $E_{1/2}^{\text{Ox2}}$ | $E_{1/2}^{\text{Ox1}}$ | K_c^b | $E_{1/2}^{\text{Red1}}$ | $E_{1/2}^{\text{Red2}}$ |
|------------|------------------------|------------------------|-------------------|-------------------------|-------------------------|
| 2^{2+} | 0.37 | -0.11 | 1.3×10^8 | -1.29 | -1.73 |
| $4^{2+,c}$ | 0.77 | 0.36 | 7.9×10^6 | -1.15 | n.o. ^d |

^aHalf-wave potentials in V from cyclic voltammetry in $\text{CH}_2\text{Cl}_2/0.1$ M Bu_4NPF_6 at 298 K. Scan rate: 100 mV/s. Decamethylferrocene/decamethylferrocenium was used as an internal standard, and the potentials were referenced against ferrocene/ferrocenium by using literature values.²⁶ ^b $K_c = 10^{\Delta E/59}$, $\Delta E = E_{1/2}^{\text{Ox2}} - E_{1/2}^{\text{Ox1}}$. ^cData from ref 5c, corrected with appropriate referencing. ^dn.o. = not observed.

appropriate plot is shown in Figure 3. The osmium complex 2^{2+} displays two reversible oxidation and two reversible reduction processes in $\text{CH}_2\text{Cl}_2/0.1$ M Bu_4NPF_6 (Table 2 and Figure 3).

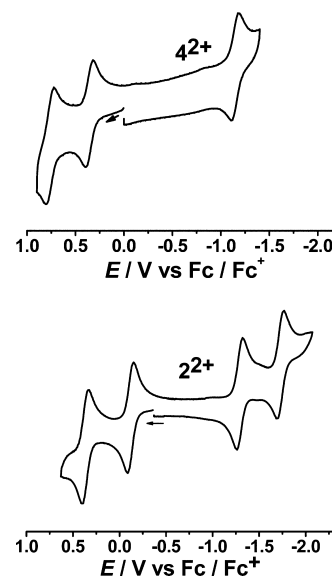


Figure 3. Cyclic voltammograms of 4^{2+} (top) and 2^{2+} (bottom) in $\text{CH}_2\text{Cl}_2/0.1$ M Bu_4NPF_6 at 295 K.

A comparison between the potentials of 2^{2+} and 4^{2+} measured under identical conditions shows some interesting trends. A look at Table 2 shows that all potentials for 2^{2+} containing the higher homologue osmium are cathodically shifted compared to 4^{2+} . This is to be expected because of the better π -donor ability of osmium in comparison to ruthenium.¹⁷ However, the shifts of the potentials for the individual redox processes are not uniform. Thus, whereas the first oxidation potential for 2^{2+} is -0.11 V, the corresponding value for 4^{2+} is 0.36 V; a look at the first reduction potentials shows the values for 2^{2+} and 4^{2+} at -1.29 and -1.15 V, respectively. This large shift for the oxidation potentials and only a small change in the reduction potentials on moving from 2^{2+} to 4^{2+} are the first indications of greater metal contribution to the oxidation processes in comparison to the reduction processes (see below).

The difference in half-wave potentials of the two oxidation processes for 2^{2+} is larger than that for 4^{2+} . This larger potential difference translates into a comproportionation constant, K_c ,¹⁸ about 2 orders of magnitude higher for 2^{2+} in comparison to 4^{2+} (Table 2). Since electrochemical measurements for both the complexes were carried out in the same solvent and electrolyte under identical conditions, the difference in the thermodynamic stabilities of the one-electron-oxidized species can be attributed

to electronic differences between the two complexes. Considering a superexchange mechanism, valence exchange between the metal centers would take place via the π^* orbital of the bridging ligand. Stronger binding of the Os(II) and Os(III) ions to the bridging ligand enforce donor–bridge–acceptor interactions and stabilize the mixed-valence state to a greater degree than in the case of ruthenium.¹⁷

UV–Vis–Near-IR and EPR Spectroelectrochemistry.

The Ru–arene complex **3** displays an absorption band at 526 nm (Table 3), which is tentatively assigned to a Ru ($d\pi$) to L_{2H}

Table 3. UV–Vis–Near-IR Data of the Complexes^a

| compd | λ_{\max}/nm ($\epsilon/M^{-1}\text{cm}^{-1}$) |
|-----------------------|--|
| 1^+ | 393 (1550), 590 (1330), 731 (2800), 1275 (470) |
| 1 | 394 (1580), 582 (2950) |
| 2^{4+} | 519 (6800), 682 (12900), 908 sh, 1657 (1090) |
| 2^{3+} | 441 (4630), 792 (15200), 1251 (1030), 1568 (770), 1983 (910) |
| 2^{2+} | 400 (6420), 721 (10900), 793 (11500), 884 (10700), 1129 sh |
| 2^+ | 400 (6190), 549 (4790), 927 (6960), 1133 sh |
| 3 | 327 (12400), 433 sh, 526 (20100) |
| 4^{4+} ^b | 528, 760 |
| 4^{3+} ^b | 390, 524, 716, 830 sh, 1287, 1674 sh |
| 4^{2+} ^b | 369, 661 sh, 707 |
| 4^+ ^b | 327, 429, 558, 737 sh, 858, 964 sh |

^aMeasurements in $\text{CH}_2\text{Cl}_2/0.1\text{ M Bu}_4\text{NPF}_6$ (OTTLE spectroelectrochemistry). ^bExtinction coefficients could not be determined accurately because of the poor solubility of the compound.

(π^*) metal to ligand charge transfer (MLCT) transition. On moving to the osmium analogue **1**, this band is shifted to 582 nm (Table 3 and Figure 4). The shift of the MLCT band of **1**

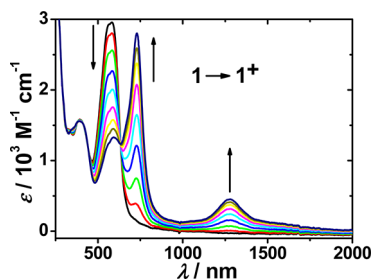


Figure 4. Changes in the UV–vis–near-IR spectrum of **1** in $\text{CH}_2\text{Cl}_2/0.1\text{ M Bu}_4\text{NPF}_6$ during the first oxidation.

to lower energy in comparison to **3** can be rationalized by the better π -donor properties of Os(II) in comparison to Ru(II), which would lead to a destabilization of the metal-based orbitals in **1** in comparison to **3**.¹⁷ Both **1** and **3** show other bands at higher energy (Table 3) that are intraligand in origin. The completely irreversible nature of the cyclic voltammogram of **3** precluded the spectroscopic characterization of the other redox states of **3**.

On one-electron oxidation of **1** to 1^+ using an optically transparent thin-layer electrochemical (OTTLE) cell,¹⁹ the MLCT band at 582 nm loses intensity, and a new band appears at 731 nm (Figure 4 and Table 3). This band is assigned to a ligand to metal charge transfer (LMCT) transition. A redox-active ligand such as L_{2H} is expected to have filled orbitals close in energy to the metal-based orbitals, and hence this assignment seems plausible. In addition, 1^+ shows a band in the near-IR region at 1275 nm with an extinction coefficient of 470 M^{-1}

cm^{-1} . Since **1** does not display any other oxidation waves within the dichloromethane solvent window, it is not possible to probe if this band might disappear after a second oxidation. The results of DFT calculations (detailed below) nevertheless provide evidence for strong electronic coupling. The in situ electrochemically generated one-electron-oxidized form 1^{1+} turned out to be EPR silent down to liquid-nitrogen temperatures. This can be taken as an evidence of a metal-centered oxidation, because a heavy 5d element such as osmium, with its large spin–orbit coupling constant (3000 cm^{-1} for Os^{III}),²⁰ would lead to fast relaxation pathways and broadening of EPR lines beyond detection.²¹ By putting together the results described above, 1^+ can be tentatively assigned as a mixed-valence species. The experimental $\Delta\nu_{1/2}$ value for the band at 1275 nm is 964 cm^{-1} . On using the Hush formulation $\sqrt{(2310\nu_{\max})}$,²² the calculated $\Delta\nu_{1/2}$ value turns out to be 4256 cm^{-1} . The larger calculated bandwidth at half-height in comparison to the experimental value indicates that 1^+ belongs to the strongly coupled class III mixed-valent systems in the Robin and Day classification scheme. Class III character, despite the weak intensity of near-IR bands, has previously been observed for other systems.^{12a}

4^{2+} displays a main MLCT band at 707 nm (Table 3 and Figure 5). On moving to the osmium analogue 2^{2+} , the MLCT band(s) is shifted to lower energy (Table 3 and Figure 6), as has been observed for **1** in comparison to **3**. The MLCT band is split into three different bands for both complexes. The effect

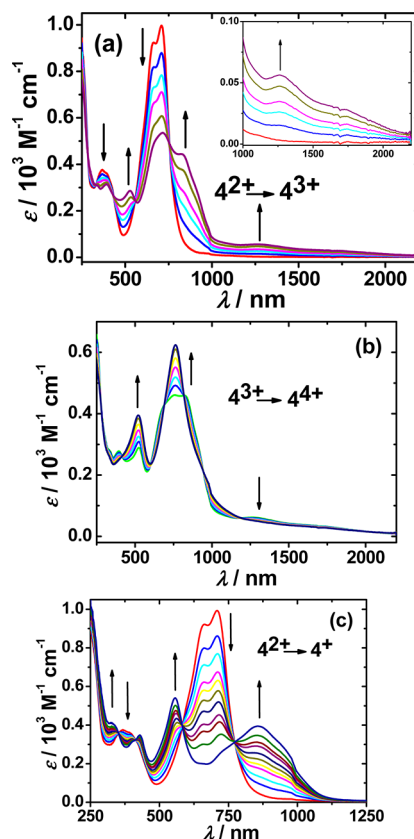


Figure 5. Changes in the UV–vis–near-IR spectrum of 4^{2+} in $\text{CH}_2\text{Cl}_2/0.1\text{ M Bu}_4\text{NPF}_6$ during the (a) first oxidation (the inset shows changes in the region 1000–2250 nm), (b) second oxidation, and (c) first reduction.

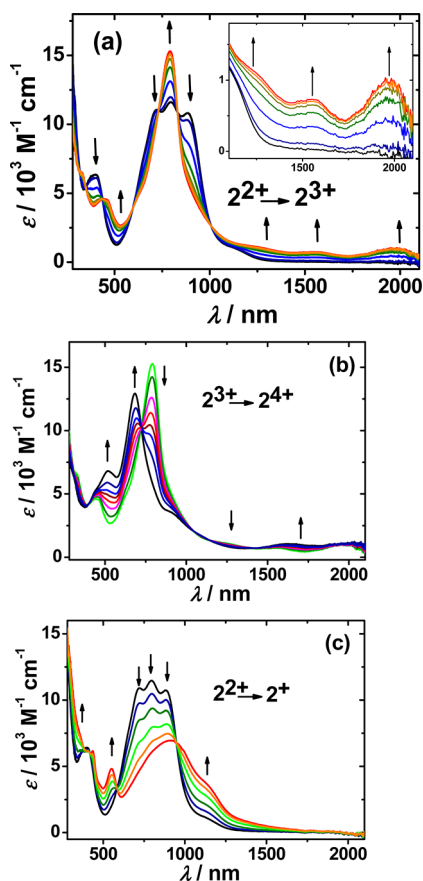


Figure 6. Changes in the UV-vis-near-IR spectrum of 2^{2+} in $\text{CH}_2\text{Cl}_2/0.1 \text{ M Bu}_4\text{NPF}_6$ during the (a) first oxidation (the inset shows changes in the region 1000–2250 nm), (b) second oxidation, and (c) first reduction.

is more prominent for the osmium complex, possibly due to a larger vibronic coupling in the osmium complex 2^{2+} .^{12c,23}

On one-electron oxidation to 4^{3+} , the band at 707 nm loses intensity and a new band appears at 830 nm. This band is assigned to a LMCT transition. 4^{3+} also displays an absorption in the near-IR region at 1287 nm. This band disappears on further oxidation to 4^{4+} . As has been reported previously by us,^{5c} the in situ electrochemically generated species 4^{3+} is EPR silent at room temperature. At 110 K 4^{3+} shows an EPR signal with an average g value of 2.065 and a g anisotropy of 0.168 (Table 4). The deviation of the average g value from the free electron g value of 2.0023 and the substantial g anisotropy are an indication of spin at the metal centers.²⁴ Taking the UV-vis-near-IR and EPR data together, 4^{3+} can be assigned as a mixed-valence diruthenium species. The experimental $\Delta\nu_{1/2}$ value for the band at 1287 nm is 942 cm^{-1} ; on using the Hush

Table 4. EPR Data of the Complexes^a

| compd | g_1 | g_2 | g_3 | Δg^b | g_{av}^d |
|---------------|-------|-------|-------|--------------|-------------------|
| $2^+{}^c$ | | | | | 1.982 |
| 2^{3+} | 2.355 | 2.128 | 1.915 | 0.440 | 2.140 |
| $4^+{}^{c,e}$ | | | | | 1.998 |
| $4^{3+}{}^e$ | 2.143 | 2.074 | 1.975 | 0.168 | 2.065 |

^aEPR data of in situ generated species in $\text{CH}_2\text{Cl}_2/0.1 \text{ M Bu}_4\text{NPF}_6$. ^b $\Delta g = g_1 - g_3$. ^cIsotropic g values for measurements at 295 K. ^dFor 2^{3+} and 4^{3+} , $g_{\text{av}} = \sqrt{(g_1^2 + g_2^2 + g_3^2)/3}$. ^eFrom ref 5c.

equation ($\sqrt{(2310\nu_{\text{max}})^2}$),²² the calculated $\Delta\nu_{1/2}$ value is 4236 cm^{-1} , indicating that 4^{3+} belongs to the strongly coupled class III mixed-valent species [$\text{Ru}(2.5)\text{--Ru}(2.5)$].

When the osmium complex is oxidized to 2^{3+} , several bands appear in the visible and near-IR region. For a mixed-valent formulation, apart from the MLCT or LMCT bands, several interconfiguration and intervalence charge transfer bands are possible and allowed for osmium complexes, as has been pointed out in an excellent review article.²³ Of the various bands in the near-IR region, that at 1251 nm (Table 3 and Figure 6) disappears on further oxidation to 2^{4+} . 2^{3+} is EPR silent at room temperature. At 110 K, 2^{3+} shows an EPR signal with an average g value of 2.140 and a reasonably large g anisotropy of 0.440 (Table 4 and Figure 7). Both the average g

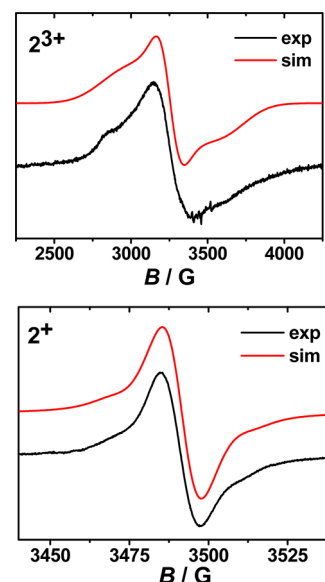


Figure 7. X-band EPR spectrum of in situ electrochemically generated 2^{3+} at 110 K (top) and 2^+ at 295 K (bottom) in $\text{CH}_2\text{Cl}_2/0.1 \text{ M Bu}_4\text{NPF}_6$.

value and the g anisotropy are substantially larger for the odd-electron osmium complex 2^{3+} in comparison to its ruthenium counterpart 4^{3+} . These results are probably a combined effect of more spin density on the metal centers for 2^{3+} as well as the higher spin-orbit coupling constant for osmium as compared to ruthenium.²⁰ The appearance of an EPR signal at 110 K for 2^{3+} but not for 1^+ , despite both being diosmium complexes, points to different electronic situations and a more facile relaxation pathway for 1^+ in comparison to 2^{3+} . The combined UV-vis-near-IR and EPR investigations suggest that 2^{3+} is a mixed-valent species. Analysis of the band at 1251 nm reveals an experimental $\Delta\nu_{1/2}$ value of 480 cm^{-1} ; the calculated $\Delta\nu_{1/2}$ value according to Hush²² is 4297 cm^{-1} , indicating that 2^{3+} , like 1^+ and 4^{3+} , belongs to the strongly coupled class III mixed-valent species.

On one-electron reduction to 4^+ , the MLCT band is shifted to higher energy, and a new low-energy band appears at 858 nm, which is assigned to an LMCT transition. 4^+ shows a narrow EPR signal at 295 K centered at $g = 1.998$, as reported previously.^{5c} The appearance of the signal at room temperature and the small deviation of the g value from the free electron g value are indications of the unpaired electron residing in a predominantly ligand-centered orbital.²⁴ The one-electron

reduction of 4^{2+} thus leads to a reduction of the L_{2H} ligand in that molecule.

Just as for the ruthenium case, the one-electron reduction of the osmium compound to 2^+ shifts the MLCT band to higher energy and leads to the emergence of a new low-energy band at 927 nm, which is assigned to a LMCT transition (Figure 6 and Table 3). 2^+ shows an EPR signal at 295 K centered at $g = 1.982$. This spectrum could be simulated with hyperfine coupling to osmium (osmium satellites)²⁰ of 13 G. The appearance of an EPR signal at room temperature despite the presence of a 5d metal center, the small deviation of the g value from the free electron g value, and the relatively small hyperfine coupling constant to osmium are indications of a ligand-centered reduction.²⁴ Thus, just as for 4^+ , 2^+ has its spin predominantly located on the L_{2H} bridging ligand. The second reduction of 2^{2+} was not completely reversible on the spectroelectrochemistry time scale and hence cannot be discussed here.

DFT Calculations. Structure-based DFT calculations using the functionals B3LYP was used to calculate spin density distributions for the paramagnetic forms of the metal complexes. A look at the spin densities calculated according to Löwdin population analysis shows that for 1^+ more than 60% spin density is located at the osmium centers (Figure 8). This result indirectly reinforces the assignment of the near-IR band observed for 1^+ as an indication of this being a mixed-valent species (vide supra).

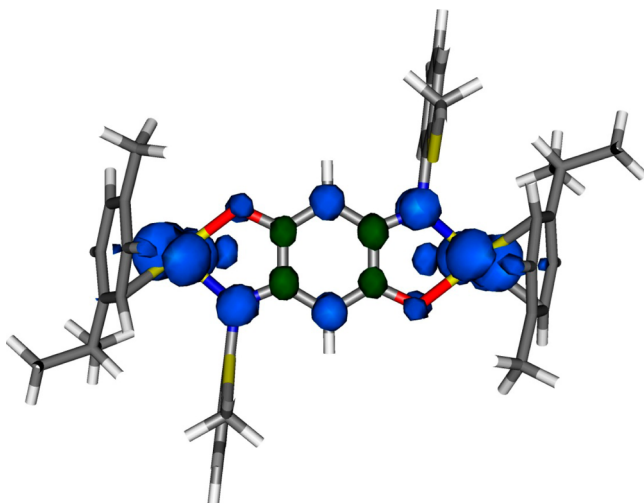


Figure 8. DFT calculated spin density plot of 1^+ . Each osmium atom accounts for 31% of the spin population.

For the one-electron-oxidized form 2^{3+} , a total of more than 60% spin density is localized on the osmium centers. In contrast, for the reduced form 2^+ , the spin density on the osmium centers is negligible (Figure 9). These results thus corroborate the assignments made from spectroelectrochemistry measurements of 2^{3+} being a mixed-valent species with predominantly osmium-centered spin and 2^+ being a ligand-radical-bridged diosmium(II) species with almost exclusive ligand-centered spin. The corresponding spin density distributions for the ruthenium complexes show slightly more than 50% spin densities on the ruthenium centers for 4^{3+} and almost negligible spin densities on the metal centers for 4^+ (Figure S3, Supporting Information).

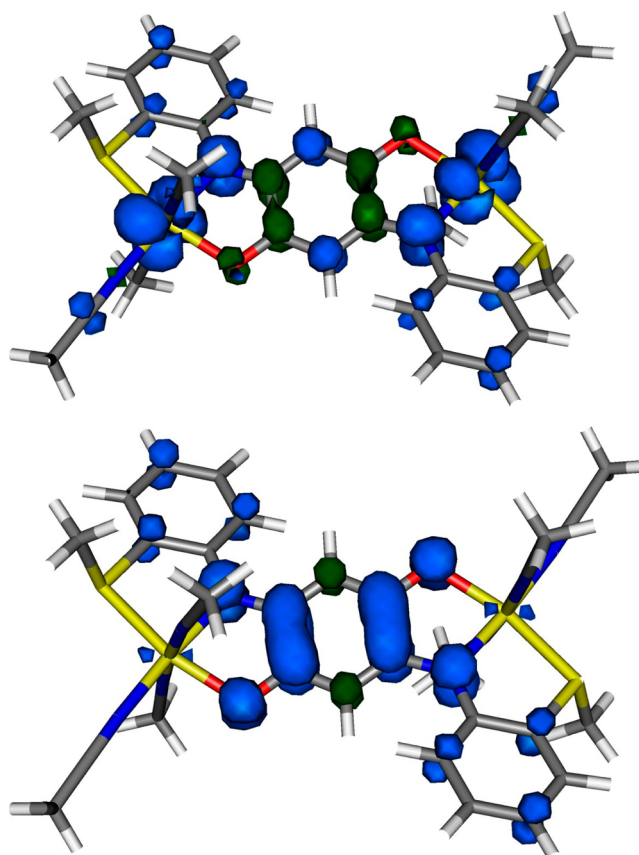


Figure 9. DFT calculated spin density plot of 2^{3+} (top; each osmium atom accounts for 32% of the spin population) and 2^+ (bottom).

CONCLUSIONS

In conclusion, we have presented here the synthesis and characterization of two quinonoid-bridged diosmium complexes. The arene–osmium-containing complex **1** displays a substituent-induced reactivity on chloride abstraction, which leads to the coordination of the thioether groups of the bridging ligand to the osmium centers and to arene release. This set of chemical transformations leads to the acetonitrile-containing complex 2^{2+} , where the bridging ligand acts in a “bis-tridentate” fashion. Comparison of **1** and 2^{2+} with their ruthenium analogues **3** and 4^{2+} reveals the more robust nature of the osmium–ligand bonds, leading to higher reaction times and temperatures for the osmium compounds in comparison to their ruthenium analogues. The diosmium complex 2^{2+} displays a higher comproportionation constant in comparison to its diruthenium analogue. Electrochemical and UV–vis–near-IR spectroelectrochemical investigation of **1** and 2^{2+} shows a predominantly metal-centered oxidation for both of these compounds, resulting in the generation of completely delocalized class III mixed-valence species in the odd-electron oxidized form. Metal contribution to the singly occupied molecular orbital (SOMO) is higher for 2^{3+} in comparison to the analogous ruthenium compound 4^{3+} . This is evident from much larger g anisotropy for 2^{3+} in comparison to 4^{3+} . The one-electron reduction of 2^{2+} leads to the reduction of the bridging quinone and the generation of a ligand-radical-bridged homovalent diosmium(II) complex. Spin density calculations corroborate the assignments made on the basis of spectroelectrochemical experiments. The UV–vis–near-IR spectra of the osmium complexes are complicated by the presence of many

bands in the visible and near-IR region because of the observance of forbidden transitions in case of the 5d metal center. We note here that the use of potentially bridging quinones that contain additional donor atoms on their nitrogen substituents is rare in the literature. Ligand-bridged diosmium complexes have also been much less investigated in comparison to their diruthenium counterparts. We have presented here examples of two new diosmium complexes by combining both of these concepts. Additionally, the arene–osmium complex presented here displays reversible electrochemical responses. This is in contrast to their ruthenium counterparts known in the literature.¹⁰ Hence, the use of arene–osmium components might deliver rectangles and cages better suited for redox-switching and redox-sensing studies.

■ EXPERIMENTAL SECTION

General Considerations. $[\text{Os}(\text{Cym})_2\text{Cl}_2]_2$ ¹³ and the ligand **L**^{5c} were prepared according to reported procedures. All other reagents are commercially available and were used as received. All solvents were dried and distilled using common techniques unless otherwise mentioned.

Instrumentation. ¹H NMR spectra were recorded at 250.13 MHz on a Bruker AC250 instrument. EPR spectra in the X band were recorded with a Bruker System EMX instrument. Simulations of EPR spectra were done using the Easyspin program.²⁵ UV–vis–near-IR absorption spectra were recorded on a J&M TIDAS spectrometer. Cyclic voltammetry was carried out in 0.1 M Bu₄NPF₆ solutions using a three-electrode configuration (glassy-carbon working electrode, Pt counter electrode, Ag wire as pseudoreference) and PAR 273 potentiostat and function generator. The decamethylferrocene/decamethylferrocenium couple served as internal reference, and the values were then converted to the ferrocene/ferrocenium couple as standard by using literature values.²⁶ Spectroelectrochemical measurements were carried out using an optically transparent thin-layer electrochemical (OTTLE) cell consisting of platinum-grid working and auxiliary electrodes and a silver quasi-reference electrode sealed between optical windows.¹⁹ The cell was mounted on the J&M TIDAS diode-array spectrometer, and the spectra were collected continuously during the potential scan within the redox steps. Elemental analysis was performed on a Perkin-Elmer Analyzer 240 instrument. Mass spectrometry experiments were carried out on a Bruker Daltonics Microtof-Q mass spectrometer.

Synthesis. $[\{\text{Cl}(\eta^6\text{-Cym})\text{Os}\}_2(\mu\text{-}\eta^2\text{-}\eta^2\text{-L-2H})] \text{ (1)}$. Os₂(Cym)₂Cl₄ (80.0 mg, 0.10 mmol) and the ligand **L** (38.0 mg, 0.10 mmol) were dissolved in CH₂Cl₂ (20 mL) under an argon atmosphere. NEt₃ (0.1 mL) was added, and the solution was stirred overnight at room temperature. The solution was concentrated, and the product was precipitated by addition of hexane. The compound was filtered, washed with hexane, and dried in vacuo. The compound was obtained as a reddish purple solid (94 mg, 85%). Anal. Calcd for C₄₀H₄₄Cl₂N₂O₂Os₂S₂: C, 43.66; H, 4.03; N, 2.55. Found: C, 43.50; H, 4.03; N, 2.70. HRMS (ESI): calcd for C₄₀H₄₄N₂O₂Os₂S₂ ([M – 2Cl]²⁺) *m/z* 515.1018; found 515.1043. ¹H NMR (400 MHz, CD₃CN): δ 1.09 (d, ³J_{H–H} = 6.9 Hz, 6H, CH(CH₃)₂), 1.13 (d, ³J_{H–H} = 6.9 Hz, 6H, CH(CH₃)₂), 1.90 (s, 6H, CH₃), 2.55 (s, 6H, SCH₃), 2.91 (sept, ³J_{H–H} = 6.8 Hz, 2H, CH(CH₃)₂), 4.93 (s, 2H, quinone-H), 5.38 (d, ³J_{H–H} = 5.5 Hz, 2H, arene-H), 5.65 (d, ³J_{H–H} = 5.3 Hz, 2H, arene-H), 5.69 (d, ³J_{H–H} = 5.4 Hz, 2H, arene-H), 5.83 (d, ³J_{H–H} = 5.6 Hz, 2H, arene-H), 7.23 (2, ³J_{H–H} = 4.0 Hz, 4H, aryl-H), 7.34 (m, 2H, aryl-H), 7.44 (d, ³J_{H–H} = 7.9 Hz, 2H, aryl-H).

$[\{\text{CH}_3\text{CN}\}_3\text{Os}\}_2(\mu\text{-}\eta^3\text{-}\eta^3\text{-L-2H})][\text{BPh}_4]_2 \text{ (2[BPh}_4\text{])}$. Compound **1** (120 mg, 0.11 mmol) and AgBF₄ (53 mg, 0.27 mmol) were dissolved in acetonitrile (40 mL) and refluxed for 19 h under an inert atmosphere of argon. After it was cooled to room temperature, the reaction mixture was filtered and the solvent was removed under reduced pressure. The resulting green solid was purified by flash column chromatography (aluminum oxide + 5 wt % water). The green 2[BF₄]₂ was eluted with CH₃CN/CH₃OH (97/3). Evaporation of the solvent

under reduced pressure gave 2[BF₄]₂ as a green solid. Anion exchange with excess NaBPh₄ gave the pure green product (40 mg, 22%). Crystals were obtained by slow diffusion of diethyl ether into an acetonitrile/toluene (1/1) solution of 2[BPh₄]₂. Anal. Calcd for C₈₇H₈₂B₂N₈O₂Os₂S₂ (M + toluene): C, 60.13; H, 4.76; N, 6.45. Found: C, 60.21; H, 5.01; N, 6.14. HRMS (ESI): calcd for C₂₄H₂₂N₄O₂Os₂S₂²⁺ ([M – 4CH₃CN – 2BPh₄]²⁺) 422.0186; found 422.0191. ¹H NMR (250 MHz, CD₃CN): δ 2.42–2.44 (m, 12H, 2 CH₃CN trans), 2.71 (s, 6H, CH₃CN), 2.87 (s, 6H, SCH₃), 6.84 (t, ³J_{H–H} = 7.1 Hz, 8H, aryl-H BPh₄[–]), 6.92 (s, 2H, quinone-H), 6.99 (t, ³J_{H–H} = 7.2 Hz, 16H, aryl-H BPh₄[–]), 7.20–7.30 (m, 18H, 16 aryl-H, BPh₄[–], 2 aryl-H), 7.43 (dt, ³J_{H–H} = 7.9 Hz, ⁴J_{H–H} = 1.5 Hz, 2H, aryl-H), 7.73 (dd, ³J_{H–H} = 7.8 Hz, ⁴J_{H–H} = 1.3 Hz, 2H, aryl-H), 8.14 (d, ³J_{H–H} = 8.2 Hz, 2H, aryl-H).

X-ray Crystallography. Single crystals of 2[BPh₄]₂ were grown by slow diffusion of diethyl ether into an acetonitrile/toluene (1/1) solution of 2[BPh₄]₂. The X-ray intensity data for 2[BPh₄]₂ were collected at 100 K using a Bruker Kappa Apex II duo diffractometer. Calculations were performed with the SHELXTL PC 5.03 and SHELXL-97 program.²⁷

The alert “PLAT413_ALERT_2_A Short Inter XH3 .. XHn H69A .. H71C .. 1.63 Ang” in the CIF-Check can be explained due to the strongly disordered toluene moiety in the structure. The refinement of the methyl group at the toluene at two different positions results in the short distance of the two protons.

CCDC 904338 contains a CIF file for 2(BPh₄)₂. These data can be obtained free of charge from the Cambridge Crystallographic Data Centre via www.ccdc.cam.ac.uk/data_requests/cif.

DFT Calculations. The program package ORCA 2.9.1 was used for all calculations.²⁸ The geometry optimization and single-point calculations were performed by the DFT method with BP86 and B3LYP functionals, respectively,²⁹ including relativistic effects in zero-order regular approximation (ZORA).³⁰ Convergence criteria for the geometry optimization were set to default values (OPT), and “tight” convergence criteria were used for SCF calculations (TIGHTSCF). Triple-ζ valence quality basis sets (def2-TZVP) were used for all atoms.³¹ The resolution of the identity approximation (RIJCOSX) was employed^{32,33} with matching auxiliary basis sets.³⁴ All spin densities were calculated according to Löwdin population analysis.³⁴ Spin densities were visualized via the program Molekel.³⁵

■ ASSOCIATED CONTENT

Supporting Information

A CIF file and table giving crystallographic data for 2[BPh₄]₂ and figures and tables giving ¹H NMR spectra, spin density plots for 4⁺⁺, and coordinates for DFT calculations. This material is available free of charge via the Internet at <http://pubs.acs.org>.

■ AUTHOR INFORMATION

Corresponding Author

*Email: biprajit.sarkar@fu-berlin.de.

Author Contributions

§Both of these authors contributed equally to this work.

Notes

The authors declare no competing financial interest.

■ ACKNOWLEDGMENTS

We are indebted to the Baden-Württemberg Stiftung and the Fonds der Chemischen Industrie (Chemiefondsstipendium for D.S.) for financial support of this work. ZEDAT, FU Berlin is acknowledged for access to the computing center. This paper is dedicated to Prof. Pierre Braunstein on the occasion of his 65th birthday, with our warm wishes.

REFERENCES

- (1) (a) Kaim, W. *Inorg. Chem.* **2011**, *50*, 9752. (b) Ward, M. D.; McCleverty, J. A. *J. Chem. Soc., Dalton Trans.* **2002**, 275. (c) Pierpont, C. G. *Coord. Chem. Rev.* **2001**, *216–217*, 95. (d) Zanello, P. G. *Coord. Chem. Rev.* **2006**, *50*, 2000. (e) de Bruin, B.; Hettterscheid, D. G. H.; Koekkoek, A. J. J.; Grützmacher, H. *Prog. Inorg. Chem.* **2007**, *55*, 247. (f) Poddel'sky, A. I.; Cherkasov, V. K.; Abakumov, G. A. *Coord. Chem. Rev.* **2009**, *253*, 291.
- (2) (a) Chaudhuri, P.; Verani, C. N.; Bill, E.; Weyhermüller, T.; Neese, F.; Wieghardt, K. *J. Am. Chem. Soc.* **2001**, *123*, 2213. (b) Bhattacharya, S.; Gupta, P.; Basuli, F.; Pierpont, C. G. *Inorg. Chem.* **2002**, *41*, 5810. (c) Mandal, S.; Paul, N.; Banerjee, P.; Mondal, T. K.; Goswami, S. *Dalton Trans.* **2010**, *39*, 2717. (d) Fabre, M.; Bonvoisin, J. *J. Am. Chem. Soc.* **2007**, *129*, 1434. (e) Sarkar, B.; Huebner, R.; Pattacini, R.; Hartenbach, I. *Dalton Trans.* **2009**, 4653. (f) Deibel, N.; Schweinfurth, D.; Fiedler, J.; Zalis, S.; Sarkar, B. *Dalton Trans.* **2011**, *40*, 9925. (g) Paretzki, A.; Das, H. S.; Weisser, F.; Scherer, T.; Bubrin, D.; Fiedler, J.; Nycz, J. E.; Sarkar, B. *Eur. J. Inorg. Chem.* **2011**, 2413. (h) Maurer, J.; Linseis, M.; Sarkar, B.; Schwederski, B.; Niemeier, M.; Kaim, W.; Zalis, S.; Anson, C.; Zabel, M.; Winter, R. F. *J. Am. Chem. Soc.* **2008**, *130*, 259.
- (3) (a) Chirik, P. J.; Wieghardt, K. *Science* **2010**, *327*, 794. (b) Ringenberg, M. R.; Kokatam, S. L.; Heiden, Z. M.; Rauchfuss, T. B. *J. Am. Chem. Soc.* **2008**, *130*, 788. (c) Praneeth, V. K. K.; Ringenberg, M. R.; Ward, T. R. *Angew. Chem.* **2012**, *124*, 10374. (d) Dzik, W. L.; van der Vlugt, J. L.; Reek, J. N. H.; de Bruin, B. *Angew. Chem.* **2011**, *123*, 3416. (e) Nguyen, A. I.; Blackmore, K. J.; Carter, S. M.; Zarkesh, R. A.; Heyduk, A. F. *J. Am. Chem. Soc.* **2009**, *131*, 3307. (f) Tsai, M. K.; Rochford, J.; Polyansky, D. E.; Wada, T.; Tanaka, K.; Muckerman, J. T. *Inorg. Chem.* **2009**, *48*, 4372. (g) Deibel, N.; Schweinfurth, D.; Hohloch, S.; Fiedler, J.; Sarkar, B. *Chem. Commun.* **2012**, *48*, 2388.
- (4) (a) Ward, M. D. *Inorg. Chem.* **1996**, *35*, 1712. (b) Leschke, M.; Melter, M.; Lang, H. *Inorg. Chim. Acta* **2003**, *350*, 114. (c) Kitagawa, S.; Kawata, S. *Coord. Chem. Rev.* **2002**, *224*, 11. (d) Carbonera, C.; Dei, A.; Letard, J.-F.; Sangregorio, C.; Sorace, L. *Angew. Chem., Int. Ed.* **2004**, *43*, 3136. (e) Müller, J. S.; Min, K. S. *Angew. Chem., Int. Ed.* **2009**, *48*, 262. (f) Therrien, B.; Süß-Fink, G.; Govindaswamy, P.; Renfrew, A. K.; Dyson, P. J. *Angew. Chem.* **2008**, *120*, 3833.
- (5) (a) Braunstein, P.; Bubrin, D.; Sarkar, B. *Inorg. Chem.* **2009**, *48*, 2534. (b) Das, H. S.; Weisser, F.; Schweinfurth, D.; Su, C.-Y.; Bogani, L.; Fiedler, J.; Sarkar, B. *Chem. Eur. J.* **2010**, *16*, 2977. (c) Schweinfurth, D.; Das, H. S.; Weisser, F.; Bubrin, D.; Sarkar, B. *Inorg. Chem.* **2011**, *50*, 1150.
- (6) (a) Bayen, S.; Barooah, N.; Sarma, R. J.; Sen, T. K.; Karmakar, A.; Baruah, J. B. *Dyes Pigm.* **2007**, *75*, 770. (b) Yang, Q.-Z.; Siri, O.; Braunstein, P. *Chem. Commun.* **2005**, 2660. (c) Yang, Q.-Z.; Siri, O.; Braunstein, P. *Chem. Eur. J.* **2005**, *11*, 7237.
- (7) (a) Kumbhakar, D.; Sarkar, B.; Maji, S.; Mobin, S.; Fiedler, J.; Aparicio, R. J.; Kaim, W.; Lahiri, G. K. *J. Am. Chem. Soc.* **2008**, *130*, 17575. (b) Keyer, T. E.; Forster, R. J.; Jayaweera, P. M.; Coates, C. G.; McGarvey, J. J.; Vos, J. G. *Inorg. Chem.* **1998**, *37*, 5925. (c) Kar, S.; Sarkar, B.; Ghumaan, S.; Janardanan, D.; van Slageren, J.; Fiedler, J.; Puranik, V. G.; Sunoj, R. B.; Kaim, W.; Lahiri, G. K. *Chem. Eur. J.* **2005**, *11*, 4901. (d) Masui, H.; Freda, A. L.; Zerner, M. C.; Lever, A. B. P. *Inorg. Chem.* **2000**, *39*, 141. (e) Das, H. S.; Das, A. K.; Pattacini, R.; Huebner, R.; Sarkar, B.; Braunstein, P. *Chem. Commun.* **2009**, 4387. (f) Cotton, F. A.; Jin, J.-Y.; Li, Z.; Murillo, C. A.; Reibenspies, J. H. *Chem. Commun.* **2008**, 211. (g) Weisser, F.; Huebner, R.; Schweinfurth, D.; Sarkar, B. *Chem. Eur. J.* **2011**, *17*, 5727. (h) Paretzki, A.; Pattacini, R.; Huebner, R.; Braunstein, P.; Sarkar, B. *Chem. Commun.* **2010**, *46*, 1497. (i) Deibel, N.; Schweinfurth, D.; Huebner, R.; Braunstein, P.; Sarkar, B. *Dalton Trans.* **2011**, *40*, 431. (j) Man, W. Y.; Xia, J.-L.; Brown, N. J.; Farmer, J. D.; Yufit, D. S.; Howard, J. A. K.; Low, P. J. *Organometallics* **2011**, *30*, 1852. (k) Xia, J. L.; Man, W. Y.; Zhu, X.; Zhang, C.; Jin, G.-J.; Schauer, P. A.; Fox, M. A.; Yu, G.-A.; Low, P. J.; Liu, S. H. *Organometallics* **2012**, *31*, 5321. (l) Shao, J.-Y.; Yang, W.-W.; Yao, J.; Zhong, Y.-W. *Inorg. Chem.* **2012**, *51*, 4343. (m) Yao, C.-J.; Yao, J.; Zhong, Y.-W. *Inorg. Chem.* **2011**, *50*, 6847.
- (8) Margraf, G.; Kretz, T.; de Biani, F. F.; Lasi, F.; Loschi, S.; Zanello, P.; Bats, J. W.; Wolf, J.; Removic-Langer, K.; Lang, M.; Prokofiev, A.; Assmus, W.; Lerner, H.-W.; Wagner, M. *Inorg. Chem.* **2006**, *45*, 1277.
- (9) (a) Zhang, D.; Jin, G.-X. *Organometallics* **2003**, *22*, 2851. (b) Scheuermann, S.; Kretz, T.; Vitze, H.; Bats, J. W.; Bolte, M.; Lerner, H. W.; Wagner, M. *Chem. Eur. J.* **2008**, *14*, 2590. (c) Hohloch, S.; Braunstein, P.; Sarkar, B. *Eur. J. Inorg. Chem.* **2012**, 546. (d) Taquet, J.-P.; Siri, O.; Braunstein, P.; Welter, R. *Inorg. Chem.* **2004**, *43*, 6944. (e) Yang, Q.-Z.; Kermagoret, A.; Agostinho, M.; Siri, O.; Braunstein, P. *Organometallics* **2006**, *25*, 5518.
- (10) (a) Jia, W.-G.; Han, Y.-F.; Lin, Y.-J.; Weng, L.-H.; Jin, G.-X. *Organometallics* **2009**, *28*, 3459. (b) Han, Y.-F.; Jia, W.-G.; Yu, W.-B.; Jin, G.-X. *Chem. Soc. Rev.* **2009**, *38*, 3419. (c) Han, Y.-F.; Li, H.; Jin, G.-X. *Chem. Commun.* **2010**, *46*, 6879. (d) Han, Y.-F.; Lin, Y.-J.; Jia, W.-G.; Jin, G.-X. *Organometallics* **2008**, *27*, 4088. (e) Han, Y.-F.; Jia, W.-G.; Lin, Y.-J.; Jin, G.-X. *Organometallics* **2008**, *27*, 5002. (f) Han, Y.-F.; Jia, W.-G.; Lin, Y.-J.; Jin, G.-X. *Angew. Chem., Int. Ed.* **2009**, *48*, 6234. (g) Paul, L. E. H.; Therrien, B.; Furrer, J. *Inorg. Chem.* **2012**, *51*, 1057. (h) Mattsson, J.; Govindaswamy, P.; Renfrew, A. K.; Dyson, P. J.; Stepnicka, P.; Süß-Fink, G.; Therrien, B. *Organometallics* **2009**, *28*, 4350.
- (11) Braunstein, P.; Naud, F. *Angew. Chem., Int. Ed.* **2001**, *40*, 680.
- (12) (a) Kaim, W.; Lahiri, G. K. *Angew. Chem., Int. Ed.* **2007**, *46*, 1778. (b) Gupta, P.; Das, A.; Basuli, F.; Castineiras, A.; Sheldrick, W. S.; Mayer-Figge, H.; Bhattacharya, S. *Inorg. Chem.* **2005**, *44*, 2081. (c) Conception, J. J.; Dattelbaum, D. M.; Meyer, T. J.; Rocha, R. J. *Philos. Trans. R. Soc. A* **2008**, *366*, 163. (d) Barrigelletti, F.; Flamigni, L.; Guardigli, M.; Juris, A.; Beley, M.; Chodorowski-Kimmes, S.; Collin, J.-P.; Sauvage, J.-P. *Inorg. Chem.* **1996**, *35*, 136.
- (13) Werner, H.; Zenkert, K. *J. Organomet. Chem.* **1988**, *345*, 151.
- (14) Elschenbroich, C. *Organometallics*; Wiley-VCH: Weinheim, Germany, 2006.
- (15) Han, Y.-F.; Lin, Y.-J.; Jia, W.-G.; Jin, G.-X. *Organometallics* **2008**, *27*, 4088.
- (16) Sarkar, B.; Kaim, W.; Fiedler, J.; Duboc, C. *J. Am. Chem. Soc.* **2004**, *126*, 14706.
- (17) Kaim, W.; Kasack, V. *Inorg. Chem.* **1990**, *29*, 4696.
- (18) (a) Creutz, C. *Prog. Inorg. Chem.* **1983**, *30*, 1. (b) Crutchley, R. J. *Adv. Inorg. Chem.* **1994**, *41*, 273.
- (19) Krejčík, M.; Danek, M.; Hartl, F. *J. Electroanal. Chem.* **1991**, *317*, 179.
- (20) Weil, J. A.; Bolton, J. R.; Wertz, J. E. *Electron Paramagnetic Resonance*; Wiley: New York, 1994; p 532.
- (21) (a) Wanner, M.; Scheiring, T.; Kaim, W.; Slep, L. D.; Baraldo, L. M.; Olabe, J. A.; Zális, S.; Baerends, E. J. *Inorg. Chem.* **2001**, *40*, 5704. (b) Waldhör, E.; Kaim, W.; Olabe, J. A.; Slep, L. D.; Fiedler, J. *Inorg. Chem.* **1997**, *36*, 2969.
- (22) Hush, N. S. *Prog. Inorg. Chem.* **1967**, *8*, 391.
- (23) Demadis, K. D.; Hartshorn, C. M.; Meyer, T. J. *Chem. Rev.* **2001**, *101*, 2655.
- (24) Patra, S.; Sarkar, B.; Mobin, S. M.; Kaim, W.; Lahiri, G. K. *Inorg. Chem.* **2003**, *42*, 6469.
- (25) Stoll, S.; Schweiger, A. *J. Magn. Reson.* **2006**, *178*, 42.
- (26) Connelly, N. G.; Geiger, W. E. *Chem. Rev.* **1996**, *96*, 877.
- (27) Sheldrick, G. M. *SHELXL-97, Program for refinement of crystal structures*; University of Göttingen, Göttingen, Germany, 1997.
- (28) Neese, F. *ORCA-an Ab Initio, Density Functional and Semiempirical Program Package, version 2.9.1*; Department of molecular theory and spectroscopy, Max Planck Institute for Bioinorganic Chemistry, Mülheim/Ruhr, Germany, January 2012.
- (29) (a) Becke, A. D. *J. Chem. Phys.* **1993**, *98*, 5648. (b) Lee, C. T.; Yang, W. T.; Parr, R. G. *Phys. Rev. B* **1988**, *37*, 785.
- (30) van Wüllen, C. *J. Chem. Phys.* **1998**, *109*, 392.
- (31) Weigend, F.; Ahlrichs, R. *Phys. Chem. Chem. Phys.* **2005**, *7*, 3297.
- (32) (a) Baerends, E. J.; Ellis, D. E.; Ros, P. *Chem. Phys.* **1973**, *2*, 41. (b) Dunlap, B. L.; Connolly, J. W. D.; Sabin, J. R. *J. Chem. Phys.* **1979**, *71*, 3396. (c) Vahtras, O.; Almlöf, J.; Feyereisen, M. W. *Chem. Phys. Lett.* **1993**, *213*, 514.

- (33) (a) Eichkorn, K.; Greutler, O. T.; Ohm, H.; Haser, M.; Ahlrichs, R. *Chem. Phys. Lett.* **1995**, *242*, 652. (b) Eichkorn, K.; Weigend, F.; Treutler, O.; Ahlrichs, R. *Theor. Chem. Acc.* **1997**, *97*, 119.
- (34) (a) Löwdin, P. O. *J. Chem. Phys.* **1950**, *18*, 365. (b) Löwdin, P. O. *Adv. Quantum Chem.* **1970**, *5*, 185.
- (35) Portmann, S. *Molekel, version 5.4.0.8*; CSCS/UNI, Geneva, Switzerland, 2009.